

Turing patterns in a diffusive Holling–Tanner predator-prey model with an alternative food source for the predator

Claudio Arancibia–Ibarra^{1,2}, Michael Bode¹, José Flores³,
Graeme Pettet¹ and Peter van Heijster¹

¹School of Mathematical Sciences, Queensland University of Technology (QUT),
Brisbane, Australia.

²Facultad de Educación, Universidad de Las Américas (UDLA),
Santiago, Chile.

³Department of Mathematics, The University of South Dakota (USD),
Vermillion, South Dakota, USA

Email: claudio.arancibia@hdr.qut.edu.au, michael.bode@qut.edu.au, Jose.Flores@usd.edu,
graeme.pettet@alumni.qut.edu.au, petrus.vanheijster@qut.edu.au.

December 18, 2019

Abstract

In this manuscript, we consider temporal and spatio-temporal modified Holling–Tanner predator-prey models with predator-prey growth rate as a logistic type, Holling type II functional response and alternative food sources for the predator. From our result of the temporal model, we identify regions in parameter space in which Turing instability in the spatio-temporal model is expected and we show numerical evidence where the Turing instability leads to spatio-temporal periodic solutions. Subsequently, we analyse these instabilities. We use simulations to illustrate the behaviour of both the temporal and spatio-temporal model.

Keywords— Modified Holling–Tanner model, Alternative food, Turing instability, Turing patterns.

1 Introduction

One of the main problems in the ecological sciences is to understand the complex dynamical behaviour of the interaction between species. These interactions are becoming increasingly important in both ecology [31, 33, 34] and applied mathematics [32, 38, 39]. The goals of the analysis of these interactions are to describe different behaviours between species, to understand their long term behaviour, and to predict how they respond to management interventions [21, 29]. Dynamic complexities in such models, and in particular the Holling–Tanner predator-prey

models, are of particular mathematical interest on both temporal [2, 3, 6] and spatio-temporal domains [8, 9, 14].

The Holling–Tanner model has been used extensively to model many real-world predator-prey interactions [34, 17, 18, 37, 19, 1, 12, 20]. For instance, Hanski *et al.* [19] used the original Holling–Tanner model to investigate the multi-annual oscillation of field vole (*Microtus agrestis*) in Fennoscandia. This oscillation is generated by the predator-prey interaction between the rodent and the least weasel (*Mustela nivalis*) and the authors postulated that the least weasel population causes a delayed density dependence and therefore an oscillation phenomenon. However, the least weasel can switch its main food source depending on the proportion of the prey density. In particular, the weasel has three main food sources available birds and birds' eggs (%5 of weasels diet), rabbit (%25 of weasels diet) and small rodents (%68 of weasels diet) [30]. This characteristic was not considered in investigations associated with the oscillation of field vole in Fennoscandia which is affected by least weasel predators [34, 17, 18, 37, 19, 1, 12, 20]. That is, these studies do not consider that since the predator is a generalist they can survive under different environments and utilise a large range of food resources. Instead of adding more species to the model, we assume that these other food sources are abundantly available [30] and model this characteristic by adding a positive constant c to the environmental carrying capacity for the predator [7]. Therefore, we have a modification to the prey-dependent logistic growth term in the predator equation, namely $K(N) = hN$ is replaced by $\bar{K}(N) = hN + c$. Additionally, there exists evidence that the amplitude of the oscillation in the predator-prey interaction is affected by geographic changes, since the predator density varies from north to south in Fennoscandia [18]. Therefore, we also allow both species to diffuse.

The model of interest is

$$\begin{aligned}\frac{\partial N}{\partial t} &= rN \left(1 - \frac{N}{K}\right) - \frac{qNP}{N+a} + D_1 \nabla^2 N, \\ \frac{\partial P}{\partial t} &= sP \left(1 - \frac{P}{hN+c}\right) + D_2 \nabla^2 P.\end{aligned}\tag{1}$$

In system (1), N and P indicate the prey and predator population sizes respectively, the predator and prey population contain logistic growth functions and the predator environmental carrying capacity is a prey dependant. Moreover, the functional response is hyperbolic in form and is referred to as a Holling Type II functional response [34, 28]. Additionally, r and s are the intrinsic growth rate for the prey and predator respectively, h is a measure of the quality of the prey as food for the predator respectively, K is the prey environmental carrying capacity, q is the maximum predation rate per capita, a is half of the saturated level and c is considered the level of predators that are fed by the alternative food. We assume all parameters to be positive and, for ecological reasons, $a < K$. The predator and prey are assumed to diffuse through the spatial domain with diffusive coefficient D_1 for the prey population respectively D_2 for the predator population and ∇^2 is the standard Laplacian operator.

The aim of this manuscript is to study the spatio-temporal dynamics of the modified Holling–Tanner predator-prey model (1). We will show that the addition of the alternative food source for the predator will lead to different Turing patterns when compared to the original Holling–Tanner model (i.e. $c = 0$ in system (1)) [9]. While the original Holling–Tanner model is singular for $N = 0$, (1) is not singular and there exist system parameters that lead to spatio-temporal periodic solutions, see for instance Figure 5 in Subsection 3.1. This is not possible for the original Holling–Tanner model [9, 25].

The temporal properties of the diffusion-free model were studied in [4, 5, 15, 16] and are briefly discussed in Section 2. In this section we also discuss the basins of attraction of the equilibrium points of the diffusion-free system. In Section 3 we determine the Turing space where the Turing patterns occur and we present numerical simulations for different types of

Turing patterns in one and two space dimension. Finally, in Section 4 we compare the Turing space to the model without alternative food as studied in [9, 25] and we discuss the ecological implications.

2 Temporal Model

In order to simplify the analysis we introduce dimensionless variables by setting $u := N/K$, $v := P/(hK)$, $S := s/r$, $C := c/(hK)$, $A := a/K$, $Q := qh/(Kr)$, $\tau := rt$, $x = X\sqrt{r/D_1}$ and $d = D_2/D_1$. By substitution of these new parameters and variables into the one-dimensional version of (1) we obtain

$$\begin{aligned}\frac{\partial u}{\partial \tau} &= uF(u, v) + \nabla^2 u = u \left((1 - u) - \frac{Qv}{u + A} \right) + u_{xx}, \\ \frac{\partial v}{\partial \tau} &= vG(u, v) + d\nabla^2 v = Sv \left(1 - \frac{v}{u + C} \right) + dv_{xx}.\end{aligned}\tag{2}$$

System (2) is defined in $u(x, t) \in \mathbb{R}_{\geq 0} \times \mathbb{R}_{\geq 0}$ and $v(x, t) \in \mathbb{R}_{\geq 0} \times \mathbb{R}_{\geq 0}$ and we first recall the stability of the equilibrium points of the diffusion-free system¹

$$\begin{aligned}\frac{du}{d\tau} &= uF(u, v), \\ \frac{dv}{d\tau} &= vG(u, v).\end{aligned}\tag{3}$$

System (3) is of Kolmogorov type, that is, the axes $u = 0$ and $v = 0$ are invariant and solutions curves initiated in the first quadrant (including the axes) stay in the first quadrant. The u nullclines are $u = 0$ and $v = (u + A)(1 - u)/Q$, while the v nullclines are $v = 0$ and $v = u + C$. Hence, the equilibrium points for this system are $(0, 0)$, $(1, 0)$, $(0, C)$ and up to two coexistence equilibrium points $P_1 = (u_1, u_1 + C)$ and $P_2 = (u_2, u_2 + C)$, where $u_1 \leq u_2$ are given by

$$u_{1,2} = \frac{1}{2} \left(H_1 \pm \sqrt{\Delta} \right) \quad \text{with } \Delta = H_1^2 + 4H_2, \quad H_1 = 1 - A - Q \quad \text{and} \quad H_2 = A - CQ.\tag{4}$$

Note that, depending on the system parameters, u_1 can be negative and both u_1 and u_2 can also be complex. In [4, 5, 15, 16] the authors proved that $(0, 0)$ is always unstable, $(1, 0)$ is always a saddle point and the stability of $(0, C)$ depends on the value of H_2 (4). If $H_2 < 0$, then the equilibrium point $(0, C)$ is a saddle point, the equilibrium point is a saddle node if $H_2 = 0$, and the equilibrium point is a stable node if $H_2 > 0$. The equilibrium point P_1 is always a saddle point (when it is located in the first quadrant), while P_2 can be a stable or unstable node, see Table 1. In particular, P_1 and $(0, C)$ exchange stability by increasing H_2 through $\Delta = 0$. Moreover, the authors proved that all solutions of (3) which are initiated in $\mathbb{R}_{\geq 0}^2$ end up in the region

$$\Phi = \{(u, v), 0 \leq u \leq 1, 0 \leq v \leq 1 + C\}.\tag{5}$$

From (4) and Table 1 we can conclude that a modification of the parameter Q changes the location of the equilibrium points P_1 and P_2 and this variation also changes the stability of the equilibrium point $(0, C)$ and P_2 . Moreover, the variation of the parameter S changes the stability of the equilibrium point P_2 . Therefore, the basins of attraction of the equilibrium points $(0, C)$ and P_2 depend on the parameters Q and S . In Figure 1 the numerical bifurcation

¹Note that a different nondimensional version of the diffusion-free system (1) was studied in [4, 5, 15, 16]

H_1	H_2	Δ	Location of P_1 and P_2	P_2 is stable if	P_2 is unstable if
> 0	< 0	> 0	$P_1, P_2 \in \Phi$	$S > \frac{(H_1 + \sqrt{\Delta})(Q - \sqrt{\Delta})}{H_1 + 2A + \sqrt{\Delta}}$	$S < \frac{(H_1 + \sqrt{\Delta})(Q - \sqrt{\Delta})}{H_1 + 2A + \sqrt{\Delta}}$
$\neq 0$	> 0	> 0	$P_1 \notin \Phi, P_2 \in \Phi$		
> 0	< 0	$= 0$	$P_1 = P_2 \in \Phi$	$S > \frac{QH_1}{H_1 + 2A}$	$S < \frac{QH_1}{H_1 + 2A}$
> 0	$= 0$	> 0	$P_1 = (0, C), P_2 \in \Phi$	$S > \frac{H_1(Q - H_1)}{1 - Q}$	$S < \frac{H_1(Q - H_1)}{1 - Q}$
$= 0$	> 0	> 0	$P_1 \notin \Phi, P_2 \in \Phi$	$S > \frac{\sqrt{H_2}(Q - 2\sqrt{H_2})}{A + \sqrt{H_2}}$	$S < \frac{\sqrt{H_2}(Q - 2\sqrt{H_2})}{A + \sqrt{H_2}}$
> 0	< 0	< 0	System (3) does not have equilibrium points in Φ		
≤ 0	≤ 0				

Table 1: Stability of the coexistence equilibrium point $P_2 = (u_2, u_2 + C)$ of system (3) as derived in [4, 5, 15, 16], with H_1 , H_2 and Δ defined in (4) and Φ in (5).

package MATCONT [11] is used to obtain the bifurcation diagram² of the diffusion-free modified Holling–Taner model (3) for the system parameters $(A, C) = (0.15, 0.28)$ fixed, see top panel of Figure 1. We choose the parameter values $(A, C) = (0.15, 0.28)$ fixed since these are the values used in [4, 5, 15, 16]. Alternatively, we could have fixed Q and changed A or C and this would have resulted in equivalent bifurcation diagrams. The bifurcation curves divide the (Q, S) -space into four different areas with different behaviour:

- **Region I** ($\Delta > 0$): the equilibrium points $(0, C)$ and P_2 are stable nodes and the stable manifold of P_1 determines the boundary of the domain of attraction of $(0, C)$ and the domain of attraction of P_2 (orange and light blue regions in Figure 1 respectively). All initial conditions initiated above this separatrix go to $(0, C)$, which represents the scaled alternative food level and represents the extinction of the prey and the persistence of the predator population, while all solutions which are initiated below the separatrix go to P_2 which represent the stabilisation of both populations.
- **Region II** ($\Delta > 0$): the equilibrium point $(0, C)$ is still a stable node, while P_2 is now an unstable node surrounded by a stable limit cycle. This limit cycle is born through a Hopf bifurcation and terminated by a homoclinic bifurcation. The stable manifold of P_1 again determines the boundary of the domain of attraction of $(0, C)$ and the domain of attraction of the stable limit cycle (yellow region in Figure 1). The stable limit cycle represents the oscillation of both populations.
- **Region III** ($\Delta > 0$): the limit cycle is terminated and the equilibrium point $(0, C)$ is a global stable node and P_2 is an unstable node. Therefore, all initial conditions go to $(0, C)$ and hence the prey goes extinct.
- **Region IV** ($\Delta < 0$): system (3) does not have equilibrium points in the first quadrant and $(0, C)$ is a global stable node. Similarly with **Region III**, all trajectories with initial conditions in the first quadrant go to $(0, C)$ and hence the prey goes extinct.
- $Q = Q^*$ ($\Delta = 0$): this form the boundary between **Regions I, II & III** and **Region IV**. On this line the equilibrium point $(0, C)$ is a stable node and the equilibrium points P_1 and P_2 collapse. So, system (3) experiences a saddle-node bifurcation (labeled SN in Figure 1) and a Bogdanov–Takens bifurcation (labeled BT in Figure 1) along this line when $S = QH_1/(H_1 + 2A)$ [16].

²The Matlab package ode45 was used to generate the data for the simulations and then the PGF package (or tikz) was used to generate the graphics format.

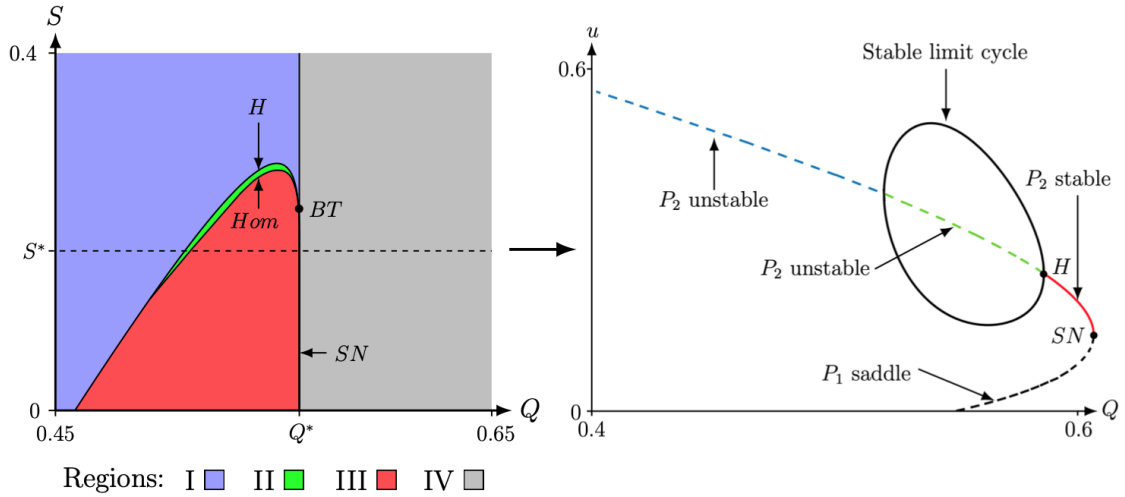


Figure 1: In the top left panel we show the bifurcation diagram of system (3) for $(A, C) = (0.15, 0.28)$ fixed and created with the numerical bifurcation package MATCONT [11]. The curve H represents the Hopf curve where P_2 changes stability and where a limit cycle is created, Hom represents the homoclinic bifurcation where the limit cycle is destroyed, SN represents the saddle-node curve where $\Delta = 0$ and BT represents the Bogdanov–Takens bifurcation. In the top right panel we show the bifurcation diagram of system (3) for $(A, C, S^*) = (0.15, 0.28, 0.23840712)$ fixed and varying the parameter Q . We show the behaviour of the equilibrium points P_1 and P_2 for different values of the parameter Q . In the phase plane of system (3) (middle and bottom panels) the orange regions represent the basin of attraction of the equilibrium point $(0, C)$, the light blue region represent the basin of attraction of the equilibrium point P_2 and the yellow region represent the basin of attraction of a stable limit cycle (only presented in Region II).

3 Spatio-temporal Model

In this section, we present the model with diffusion, we first recall the criteria for Turing instability for a general spatio-temporal predator-prey model (where the populations are assumed to be distributed in an unbounded domain)

$$\begin{aligned}\frac{\partial A}{\partial t} &= W(A, B) + \nabla^2 A, \\ \frac{\partial B}{\partial t} &= Z(A, B) + d\nabla^2 B.\end{aligned}\tag{6}$$

Here, $A(X, t)$ and $B(X, t)$ are considered to be the prey and the predator population respectively, $W(A, B)$ and $Z(A, B)$ describe their nonlinear interaction and $d = D_A/D_B$ with D_A and D_B constant diffusivities. Turing [35] showed that an equilibrium point that is stable in a temporal model can become unstable upon adding diffusion in the model. In the absence of diffusion, we analyse the stability of an equilibrium point (A_0, B_0) such that $W(A_0, B_0) = Z(A_0, B_0) = 0$. The stability of this equilibrium point depends on the eigenvalues of the Jacobian matrix $J(A_0, B_0)$ which can be found by solving $|J - \lambda I| = 0$. That is, $\lambda^2 - (W_A + Z_B)\lambda + (W_A Z_B - W_B Z_A) = 0$, where $W_A = \partial W/\partial A$, $W_B = \partial W/\partial B$, $Z_A = \partial Z/\partial A$ and $Z_B = \partial Z/\partial B$ are evaluated at the equilibrium point (A_0, B_0) . The equilibrium point (A_0, B_0) is stable if

$$\text{tr}(J(A_0, B_0)) = W_A + Z_B < 0 \quad \text{and} \quad \det(J(A_0, B_0)) = W_A Z_B - W_B Z_A > 0.\tag{7}$$

The Turing instability is obtained by linearising the PDE system around the equilibrium point (A_0, B_0) . The stability of the equilibrium point is now determined by the roots of the characteristic polynomial $|J - \lambda I - k^2 D|$ where k is the wave number [26] and $D = \begin{pmatrix} 1 & 0 \\ 0 & d \end{pmatrix}$. This defines the dispersion relation $\lambda(k)$ which is the solution of $\lambda^2 - \alpha(k^2)\lambda + \beta(k^2) = 0$ where $\alpha(k^2) = \text{tr}(J(A_0, B_0)) - k^2(1 + d)$ and $\beta(k^2) = dk^4 - (dW_A + Z_B)k^2 + \det(J(A_0, B_0))$. Hence, we obtain the dispersion relation $\lambda(k)$

$$\lambda_{\pm}(k) = \frac{1}{2} \left(\alpha(k^2) \pm \sqrt{(\alpha(k^2))^2 - 4\beta(k^2)} \right).\tag{8}$$

If we assume that the conditions defined in (7) hold then $\alpha(k^2) < 0$ and the equilibrium point (A_0, B_0) is thus unstable in (6) if we have that $\beta(k^2) < 0$. By (7) we also have that $\det(J(A, B)) > 0$ and the minimum of the quadratic $\beta(k^2)$ occurs when $k^2 = (dW_A + Z_B)/(2d)$. Therefore, the conditions for the equilibrium point (A_0, B_0) to be unstable in (6) are

$$dW_A + Z_B > 0 \quad \text{and} \quad (dW_A + Z_B)^2 - 4d \det(J(A_0, B_0)) > 0.\tag{9}$$

The Turing conditions in two-dimensional space can be obtained from (7) and (9) by replacing k^2 with $m^2 + \ell^2$, where $(m, \ell) \in \mathbb{R}^2$ indicate the wave numbers in the x -direction and y -direction respectively [8].

3.1 Equilibrium point P_2

We now discuss the Turing conditions (7) and (9) for the model of interest in this manuscript and we first focus on the coexistence equilibrium point P_2 . The only other equilibrium point that can be stable in the temporal system is $(0, C)$, we will investigate its Turing space in subsection 3.2. These Turing conditions refer to the equilibrium point P_2 to be stable in the diffusion-free system (3) and unstable in the full system (2). The conditions (7) for the equilibrium point P_2

Region	λ_0	λ_d	
(i)	< 0	< 0	$P_1 \in \Phi$ and P_2 is stable in the ODE and the PDE system
(ii)	< 0	> 0	$P_1 \in \Phi$ and P_2 is stable in the ODE system and unstable in the PDE system (Turing patterns)
(iii)	> 0	> 0	$P_1 \in \Phi$ and P_2 is unstable surrounded by a stable limit cycle in the ODE system and unstable in the PDE system
(iv)	> 0	> 0	$P_1 \in \Phi$ and P_2 is unstable without limit cycle in the ODE system and unstable in the PDE system
(v)	> 0	< 0	$P_1 \notin \Phi$ and P_2 is unstable surrounded by a stable limit cycle in the ODE system and unstable in the PDE system
(vi)	> 0	< 0	$P_1 \notin \Phi$ and P_2 is unstable without limit cycle in the ODE system and unstable in the PDE system

Table 2: Summary of the dispersion relation $\lambda(k)$ (8) of system (2) for P_2 showed in Figure 2 for system parameters $(A, C, d) = (0.15, 0.28, 5)$ fixed. There are six different cases, depending on $\lambda_0 = \mathbf{Re}(\lambda(0))$ and $\lambda_d = \max(\mathbf{Re}(\lambda(k)))$ and the potential limit cycle in the temporal system.

to be stable in the diffusion-free system are met if we assume that $H_1 > 0$, $H_2 < 0$ and $\Delta > 0$ (see Table 1). That is,

$$\frac{(H_1 + \sqrt{\Delta})(Q - \sqrt{\Delta})}{(H_1 + 2A + \sqrt{\Delta})} - S < 0 \text{ and } \frac{S(H_1 + \sqrt{\Delta})\sqrt{\Delta}}{(H_1 + 2A + \sqrt{\Delta})} > 0. \quad (10)$$

The conditions (9) for the equilibrium point P_2 to be unstable in (2) are

$$d \frac{(H_1 + \sqrt{\Delta})(Q - \sqrt{\Delta})}{(H_1 + 2A + \sqrt{\Delta})} - S > 0 \text{ and} \quad (11)$$

$$\left(\frac{d(H_1 + \sqrt{\Delta})(Q - \sqrt{\Delta})}{(H_1 + 2A + \sqrt{\Delta})} - S \right)^2 - \frac{4dS(H_1 + \sqrt{\Delta})\sqrt{\Delta}}{(H_1 + 2A + \sqrt{\Delta})} > 0.$$

Note that these assumptions on H_1 , H_2 and Δ are the most general case shown in Table 1 for which conditions (7) are met. That being said, there are other cases for which these conditions are also met, for brevity, we will not investigate these cases. Additionally, the other coexistence equilibrium point P_1 never fulfils (7) as it is a saddle point in the temporal system.

As before, we fix the system parameter $(A, C) = (0.15, 0.28)$ in system (2) and the Turing parameter space (Q, S) of the equilibrium point P_2 is given in Figure 2. Here, the conditions for the diffusion-driven instability (10) and (11) are met in region (ii) of Figure 2 and we thus expect to see Turing patterns in this region. In Table 2 we summarise the stability properties of the equilibrium point P_2 in system (2) with and without diffusion.

3.1.1 Numerical Simulations near the equilibrium point P_2

Here, we present numerical solution of system (2) in one and two-dimensional space for the system parameters $(A, C) = (0.15, 0.28)$ fixed and for initial conditions near $P_2 = (u_2 + u_2 + C)$. In particular, the initial condition is

$$u_0 = u_2 + 0.012e^{-7x^2} \quad \text{and} \quad v_0 = u_0 + C. \quad (12)$$

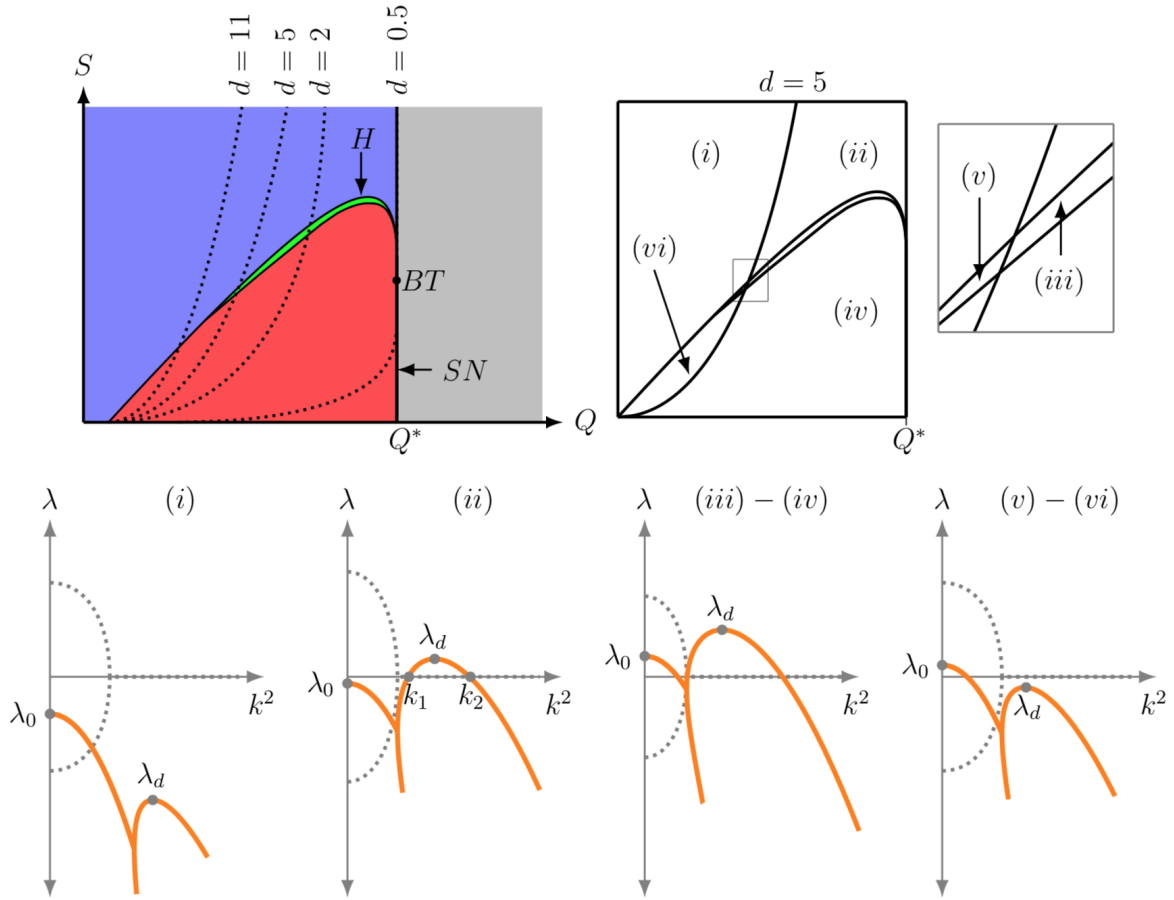


Figure 2: In the top panel we show the Turing space of system (2) for P_2 with $(A, C) = (0.15, 0.28)$ fixed. In the left top panel we consider four different values of the diffusion ratio d (0.5, 2, 5, 11) (dotted curves) and in the right top panel we consider the case where the diffusion ratio $d = 5$. In the bottom panel, we show the real part (orange curve) and imaginary part (grey dotted curve) of the dispersion relation $\lambda(k)$ (8) as a function of the wave number squared for the system parameter $(A, C, d) = (0.15, 0.28, 5)$ fixed and (i) if $Q = 0.5$ and $S = 0.27$ then P_2 is stable in the ODE and PDE system; (ii) if $Q = 0.575$ and $S = 0.26$ then P_2 is stable in the ODE and unstable in the PDE system; (iii) if $Q = 0.575$ and $S = 0.235$ or (v) if $Q = 0.52$ and $S = 0.112$ then P_2 is unstable surrounded by a stable limit cycle in the ODE system and unstable in the PDE system; (iv) if $Q = 0.575$ and $S = 0.1$ or (vi) if $Q = 0.51$ and $S = 0.18$ then P_2 is unstable without a limit cycle in the ODE system and unstable in the PDE system.

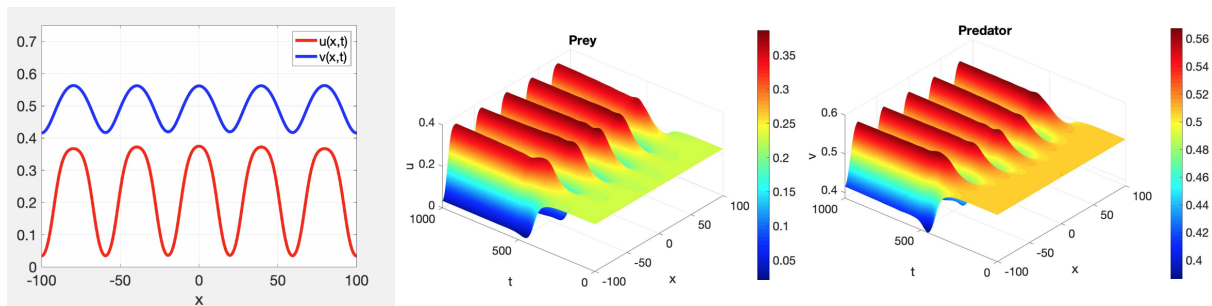


Figure 3: Numerical simulation of system (2) in one-dimensional space with system parameters $(A, C, d, Q, S) = (0.15, 0.28, 5, 0.575, 0.26)$ and initial condition defined in (12). For the parameter values the equilibrium point $P_2 = (0.22642, 0.50642)$ is unstable in the spatio-temporal system but stable in the temporal system and the formation of Turing patterns is expected, see (ii) in Figure 2. We observe a Turing pattern that is stationary in time and oscillatory in space. An animated version of this figure is accessible on <http://www.doi.org/10.6084/m9.figshare.10059242>.

The numerical integration of system (2) is performed by using the Matlab PDEPE toolbox with zero-flux boundary conditions on a domain of size 200 and we discretise using 1500 grid points. Note that increasing the domain size upon which the simulations were performed did not significantly change the observed results.

In region (i), see Figure 2 and Table 2, the equilibrium point P_2 is stable in the temporal system and in the spatio-temporal system. We observe that the initial condition (12) evolves as expected to the spatially homogeneous stationary equilibrium point P_2 (the simulation is not shown).

In region (ii), see Figure 2 and Table 2, the equilibrium point P_2 is stable in the temporal system and unstable in spatio-temporal system and the conditions for a Turing instability are thus met. Indeed, the initial condition (12) evolves to a Turing pattern that is a periodic solution in space around P_2 and that is stationary in time, see Figure 3. Note that the simulation is run over a long period of time to ensure that the Turing pattern is stationary in time. Note that the analysis of the Turing instability of Section 3.1 was based on an unbounded domain, while the numerical simulation are performed on a bounded domain. The analysis on the unbounded domain shows that there is a range of unstable wave numbers, i.e. $\mathbf{Re}(\lambda(k)) > 0$ for $k \in (k_1, k_2)$ in region (ii), see Figure 2. On a bounded domain a similar Turing analysis can be done by taking the solution as $u(x, t) = \alpha e^{\lambda t} \cos(kx)$ where α is the initial amplitude and k is the wave number. This results in a discrete set of (unstable) wave numbers lying on $\lambda(k)$ and depending on the domain size, i.e. the spatial period has to fit in the domain. In Figure 4 we show the numerical observed wave number of the Turing pattern as function of the domain size and we see that the observed wave number is as expected in between $k \in (k_1, k_2)$.

In region (iii) and (iv), see Figure 2 and Table 2, the equilibrium point P_2 is unstable with respect to wave numbers near to zero and near to λ_d . In region (iii) the equilibrium point P_2 is surrounded by a stable limit cycle in the temporal system, while this is not the case in region (iv). Note that in these two regions the equilibrium point P_1 is located in Φ and thus $(0, C)$ is a stable node in the temporal system. In region (iii), we observe that the initial condition (12) evolves to pattern that is oscillatory in space and in time, see top panel of Figure 5. Additionally, we observe that in Figure 5 the period of the oscillation in the spatio-temporal system is $40(x)$ and the wave number is $k = 0.15708$ which is in between the minimum ($k_1 = 0.135$) and maximum

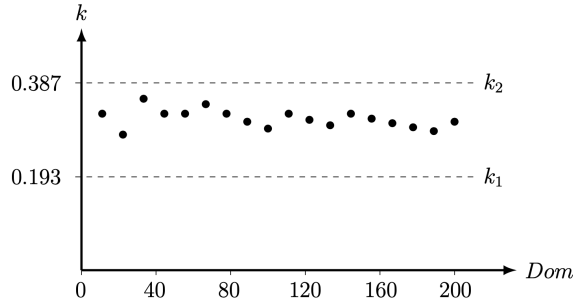


Figure 4: The numerical observed wave number of the Turing pattern as function of the domain size (Dom) for system parameters $(A, C, d, Q, S) = (0.15, 0.28, 5, 0.575, 0.26)$ fixed. We see that the observed wave numbers are in between the minimum (k_1) and maximum (k_2) for which the stable homogeneous solutions becomes unstable when diffusion is included in the model, see Figure 2.

($k_2 = 0.437$) wave number for region (*iii*), see bottom panel of Figure 2. In region (*iv*) it is observed that the initial condition (12) evolves to a different pattern that is less organised, see bottom panel of Figure 5.

In region (*v*) and (*vi*), the equilibrium point P_2 is only unstable with respect to wave numbers near zero. Additionally, in region (*v*) the equilibrium point P_2 is surrounded by a stable limit cycle in the temporal system, while there is no limit cycle in the temporal system in region (*vi*). In region (*v*), we observe that the initial condition evolves to a spatio-temporal pattern that is stationary in space and oscillatory in time, see top panel of Figure 6. We found that the period of the associated limit cycle in the temporal system is $433.3(t)$ which is close to the period of $463.787(t)$ observed in the top panel of Figure 6. In region (*vi*), we observe that the solution goes to the equilibrium point $(0, C)$.

We now shortly discuss the spatio-temporal Turing patterns of system (2) in two-dimensional space for region (*ii*) in Figure 2. We present different Turing patterns by taking system parameter $(A, C, Q, S) = (0.15, 0.28, 0.575, 0.26)$ fixed and varying the ratio of diffusivities. The numerical integration of system (2) is performed by using an Euler method for the time integration [13, 27] with a time step size $\Delta t = 0.2$ and a finite difference algorithm for a predator-prey system with spatial variation in two-dimensional Laplacian with the zero-flux boundary conditions. The initial condition is a random perturbation around the positive equilibrium point $P_2 = (0.22642, 0.50642)$. Simulations are run for a long time to ensure that the resulting patterns are stationary in time. We observe that the Turing patterns of the predator and the prey population have the same characteristics. For the ratio of diffusivity $d = 5$ we observe a stationary cold-spot pattern over the whole domain, see the top panels in Figure 7. When the ratio of diffusivity is being increased to $d = 9$ we observe that the cold-spots started to coalesce creating combination of labyrinthine and cold-spot pattern which coexist in the space, see the middle panels in Figure 7. Finally, by increasing the ratio of diffusivity up to $d = 55$ we observe a labyrinthine pattern over the whole domain, see the bottom panel in Figure 7. Moreover, we observe in Figure 7 the minimum of the prey population is 0 while the maximum increases from 0.3 up to 0.5 approximately by increasing the ratio of diffusivity. In contrast, the minimum of the predator population increases from 0.43 up to 0.48 approximately by also increasing the ratio of diffusivity while the maximum remain constant in approximately 0.55.

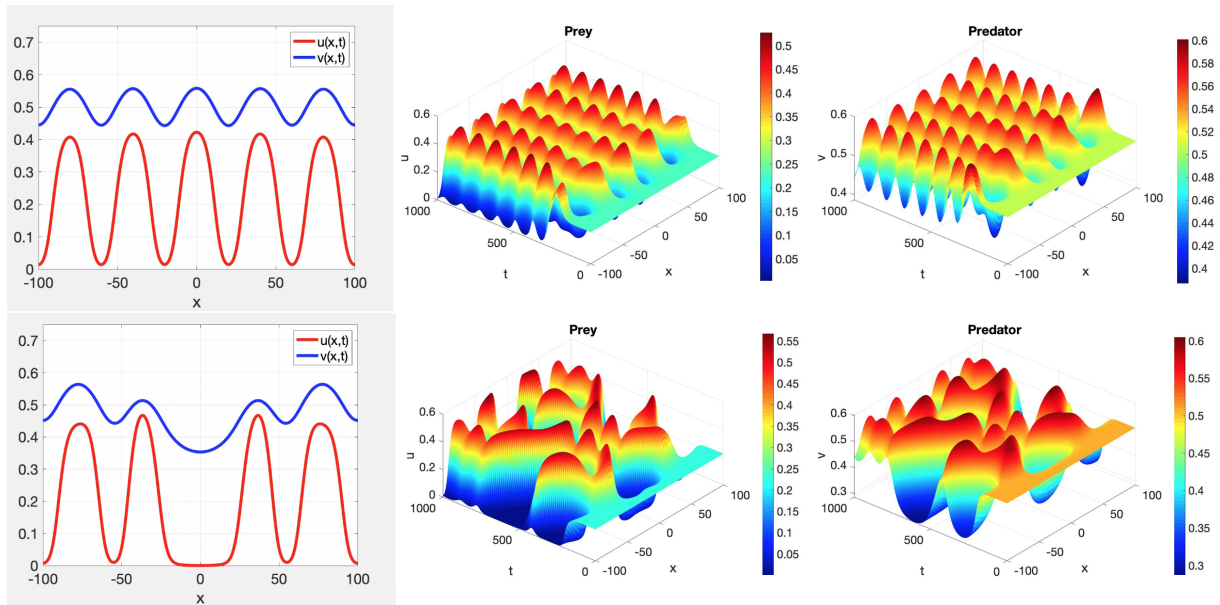


Figure 5: Numerical simulation of system (2) in one-dimensional space with system parameters $(A, C, d) = (0.15, 0.28, 5)$ fixed and initial condition defined in (12). In the top panel $(Q, S) = (0.575, 0.1)$ and the equilibrium point $P_2 = (0.22642, 0.50642)$ is unstable surrounded by stable limit cycle in the ODE system and unstable in the PDE system, see (iii) in Figure 2. We observe that the solution is oscillatory in space and in time with period $113.63(t)$ and $40(x)$ respectively. An animated version of this figure is accessible on <http://www.doi.org/10.6084/m9.figshare.10059248>. In the bottom panel $(Q, S) = (0.575, 0.07)$ and the equilibrium point P_2 is unstable and there is no limit cycle in the ODE, see (iv) in Figure 2. We observe that the solution evolves to a different pattern observed in the top panel that is less regular pattern. An animated version of this figure is accessible on <http://www.doi.org/10.6084/m9.figshare.1005925>.

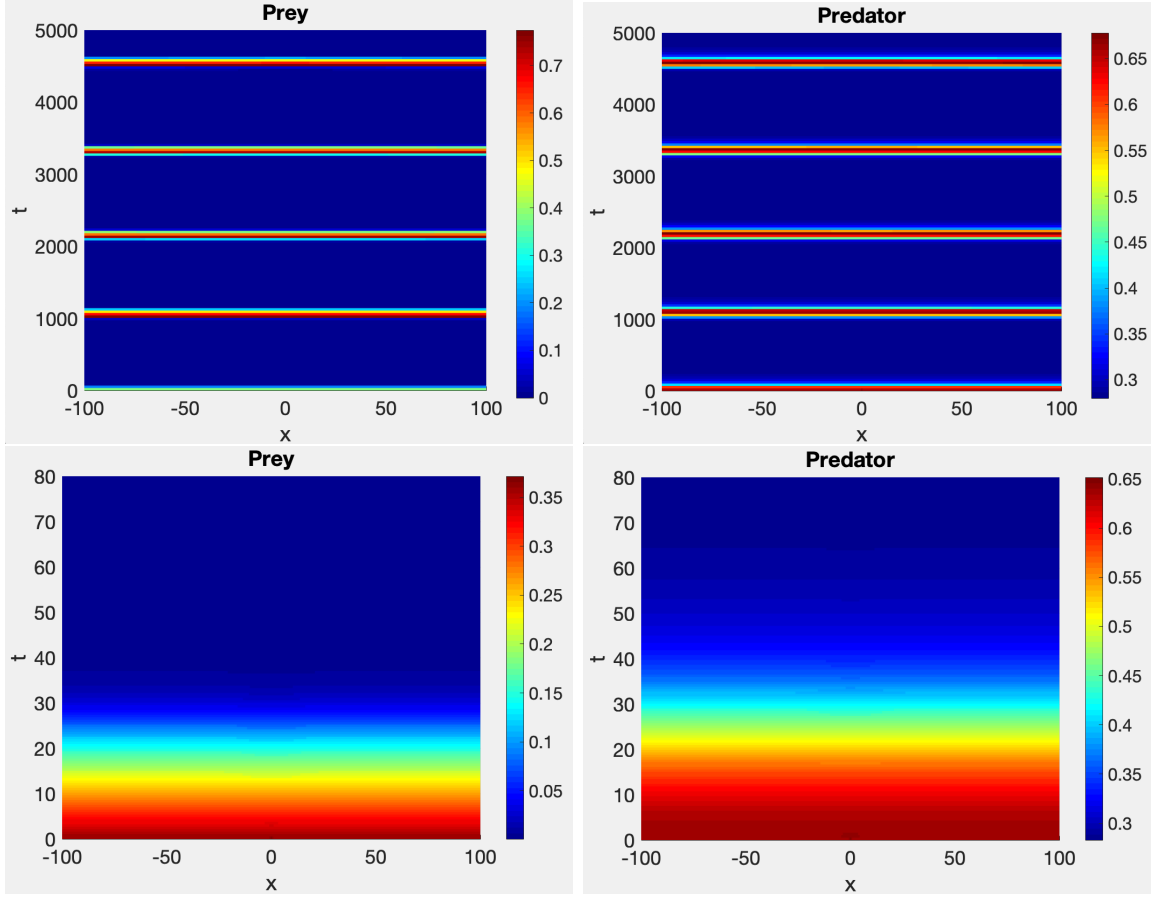


Figure 6: Numerical simulation of system (2) in one-dimensional space with system parameters $(A, C, d) = (0.15, 0.28, 5)$ fixed and initial condition defined in (12). In the top panel $(Q, S) = (0.52, 0.05)$ and the equilibrium point P_2 is unstable surrounded by stable limit cycle in the ODE system, see (v) in Figure 2. We observe the spatio-temporal pattern that is stationary in space and oscillatory in time as expected since the equilibrium point P_2 is only unstable with respect to wave numbers near zero. In the bottom panel $(Q, S) = (0.53, 0.085)$ and the equilibrium point $P_2 = (0.36, 0.64)$ is no longer surrounded by a limit cycle in the ODE system. We observe that the initial condition evolves to $(0, C)$.

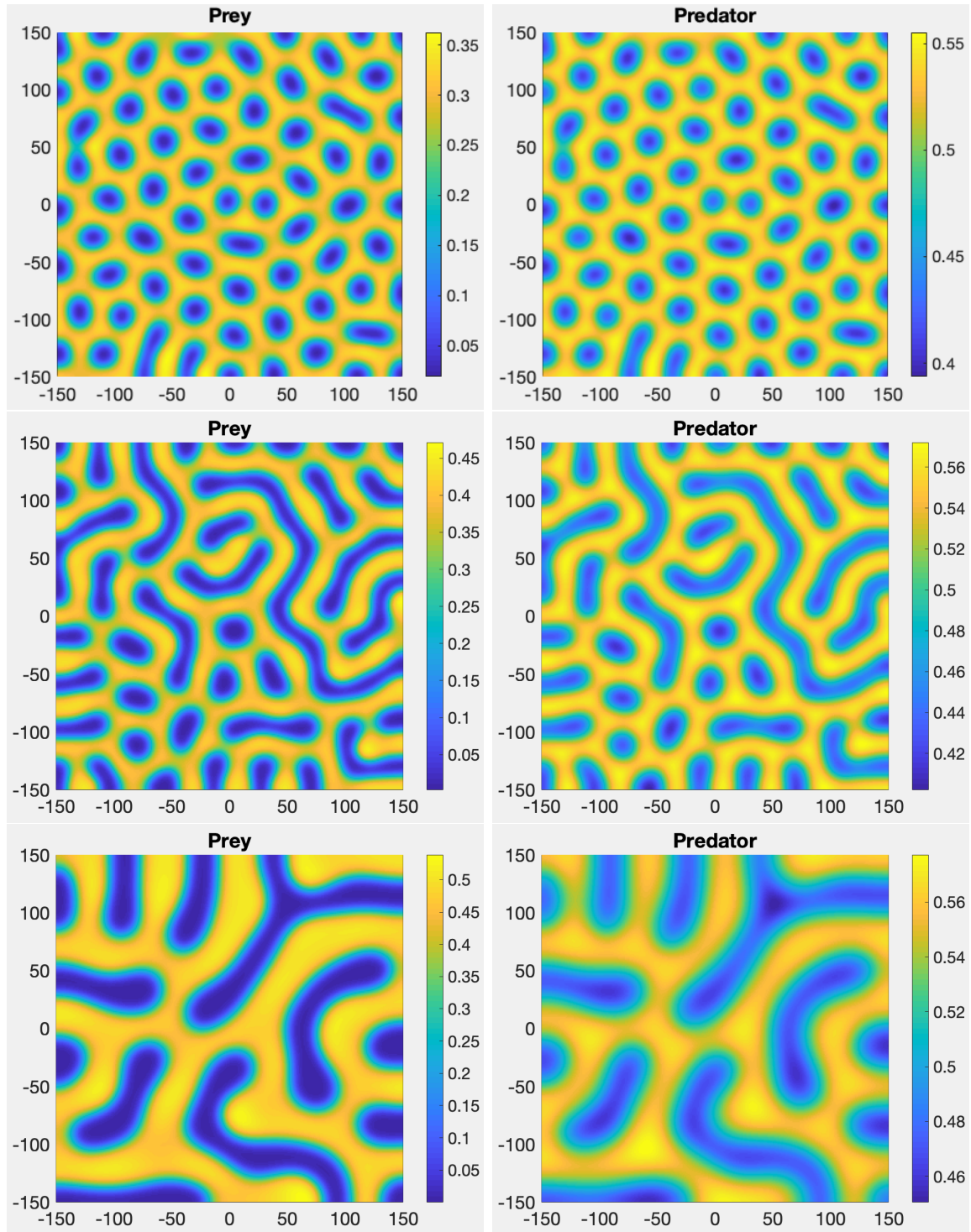


Figure 7: Numerical simulation of the predator and prey population for system (2) in two-dimensional space for initial conditions near the equilibrium point P_2 . We consider system parameters $(A, C, Q, S) = (0.15, 0.28, 0.575, 0.26)$ fixed and $d = 5$ in the top panel; $d = 9$ in the middle panel; and $d = 55$ in the bottom panel. We observe that by increasing the ratio of diffusivities the cold-spot pattern started to coalesce creating combination of labyrinthine and cold-spot pattern. Note that these Turing patterns are stationary in time.

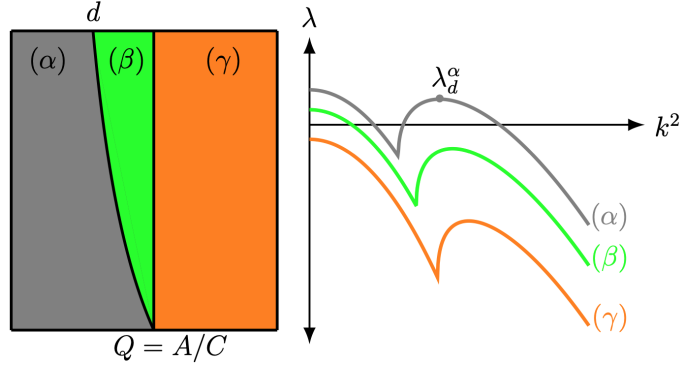


Figure 8: In the left panel we show the bifurcation diagram of system (2) for the equilibrium point $(0, C)$ with $(A, C, d) = (0.15, 0.28, 5)$ fixed. In the right panel, we show the real part of the dispersion relation $\lambda(k)$ as a function of the wave number squared for the system parameter $(A, C, d) = (0.15, 0.28, 5)$ fixed and (α) if $Q = 0.5$ and $S = 0.0701$ then $(0, C)$ is unstable with respect to small wave numbers and with respect to wave numbers near λ_d^α ; (β) if $Q = 0.55$ and $S = 0.0701$ then $(0, C)$ is unstable only with respect to small wave numbers; (γ) if $Q = 0.575$ and $S = 0.0701$ then the equilibrium point $(0, C)$ is stable in the ODE and PDE system.

3.2 Equilibrium point $(0, C)$

Next, we discuss the Turing conditions (7) and (9) for the equilibrium point $(0, C)$. The conditions in (7) for the equilibrium point $(0, C)$ are met if the system parameters are such that $H_2/A - S < 0$ and $-SH_2/A > 0$. That latter implies that H_2 should be negative since the parameters A and S are positive. The first condition in (9) for the equilibrium point $(0, C)$ is $dH_2 > AS$, but $H_2 < 0$. Therefore, the conditions (7) and (9) for the equilibrium point $(0, C)$ cannot be met simultaneously, and thus we do not expect the formation of Turing patterns near $(0, C)$. The parameters space (Q, S) of the equilibrium point $(0, C)$ is given in Figure 8 for the system parameters $(A, C) = (0.15, 0.28)$ fixed. In the grey region (α) , the equilibrium point $(0, C)$ is unstable with respect to small wave numbers and with respect to wave numbers near λ_d^α . In the green region (β) , the equilibrium point $(0, C)$ is unstable only with respect to small wave numbers, while in the orange region (γ) the equilibrium point $(0, C)$ is stable in both the ODE and PDE system.

3.2.1 Numerical Simulations of system (2) near $(0, C)$

Even though we do not expect Turing patterns, we present numerical solution to system (2) in one and two-dimensional space for the system parameters $(A, C) = (0.15, 0.28)$ fixed and initial condition near $(0, C)$. In particular, the initial condition is

$$u_0 = 0.012e^{-7x^2} \quad \text{and} \quad v_0 = u_0 + C = 0.012e^{-7x^2} + 0.28. \quad (13)$$

The numerical integration of system (2) is performed under the same conditions used in Section 3.1.1.

In region (α) , see Figure 8, the equilibrium point $(0, C)$ is unstable with respect to small wave numbers and with respect to wave numbers near λ_d^α and in (β) the equilibrium point $(0, C)$ is unstable only with respect to small wave numbers. We observe that the initial condition (13) evolves to a spatial pattern that is oscillatory in time, see top panel of Figure 9. In (γ) the

equilibrium point $(0, C)$ is stable in the ODE and PDE system. We observe that the initial condition (13) evolves, as expected, to the equilibrium point $(0, C)$, see bottom panel of Figure 9.

We also shortly discuss the spatio-temporal patterns of system (2) in two-dimensional space for region (α) in Figure 8 where the equilibrium point $(0, C)$ is unstable with respect small wave numbers and wave numbers near λ_d^α . The numerical integration of system (2) is performed under the same conditions as in Section 3.1.1 and we consider the system parameter $(A, C, Q, S) = (0.15, 0.28, 0.575, 0.26)$ fixed. The initial condition is a small random perturbation around the positive equilibrium point $(0, C) = (0, 0.28)$. For the ratio of diffusivity $d = 5$ we find cold-spot pattern over the whole domain, see left panel in Figure 10. When the ratio of diffusivity is being increased to $d = 9$ we found that the cold-spot pattern started coalescing creating combination of labyrinthine and cold-spot pattern, see the middle panel in Figure 10. Finally, by increasing the ratio of diffusivity up to $d = 55$ we observe only labyrinthine pattern over the whole domain, see the right panel in Figure 10. Note that all these patterns are stationary patterns as they remain unaltered with the further increase in time. Moreover, in Figure 10 we observe the same type of spatial pattern presented in Figure 7, however the number of cold-spot pattern is approximately double than the number of cold-spot pattern presented in Figure 10 in the same domain.

4 Conclusion

In this manuscript, we study analytically and numerically the influence of diffusion on the pattern formation of the modified Holling–Tanner model (1) with an alternative food source for the predator. We show that the pattern formation in the modified Holling-Tanner predator-prey model is rich and complex. In particular, we determine the temporal stability of the positive equilibrium point P_2 (see Table 1) and Turing instability of the same equilibrium point (see Table 2). We demonstrate the existence of a Turing instability of system (2), see region (ii) in Figure 2 and Figure 3. We show that in the neighbourhood of a Hopf bifurcation there exists a region in (Q, S) parameter space (where Q is related to the predation rate and S is related to the intrinsic growth rate for the predator) in which the dynamics exhibits spatio-temporal behaviour that is influenced by a limit cycle. Moreover, we show that there exist conditions where the distribution of species oscillate in space and time, see region (iii) in Figure 2 and top panel of Figure 5. Furthermore, the numerical simulations in two-dimensional space of system (2) show that, by increasing the diffusive constant d , the cold-spot pattern start to coalesce creating mixture Turing patterns (labyrinthine patterns and cold-spot patterns) and finally only labyrinthine patterns. The cold-spot patterns show that the prey population driven by the predator population leads to a lower proportion of the prey species in those regions. Then, by increasing the diffusive constant the population propagates in the space generating a population invasion, such that the holes connect each other forming tunnels with low population density, see Figure 7. We also determine the temporal stability of the equilibrium point $(0, C)$. We found that the Turing conditions (7) and (9) for the equilibrium point $(0, C)$ cannot be met simultaneously and therefore we do not expect the formation of Turing patterns. We observe that initial conditions evolve to spatial patterns that are oscillatory in time when (S, Q) are located in regions where a limit cycle exist, see Figure 8.

By taking the parameter $C = 0$, that is, by removing the alternative food source for the predator system (2) become singular for $u = 0$. The temporal analysis of system (2) with $C = 0$ has been studied in [32]. The authors proved the existence of a non-hyperbolic equilibrium point $(0, 0)$ and a saddle point $(1, 0)$. In addition, there is always one equilibrium point in the first quadrant and this equilibrium point can be stable, unstable surrounded by a stable limit cycle,

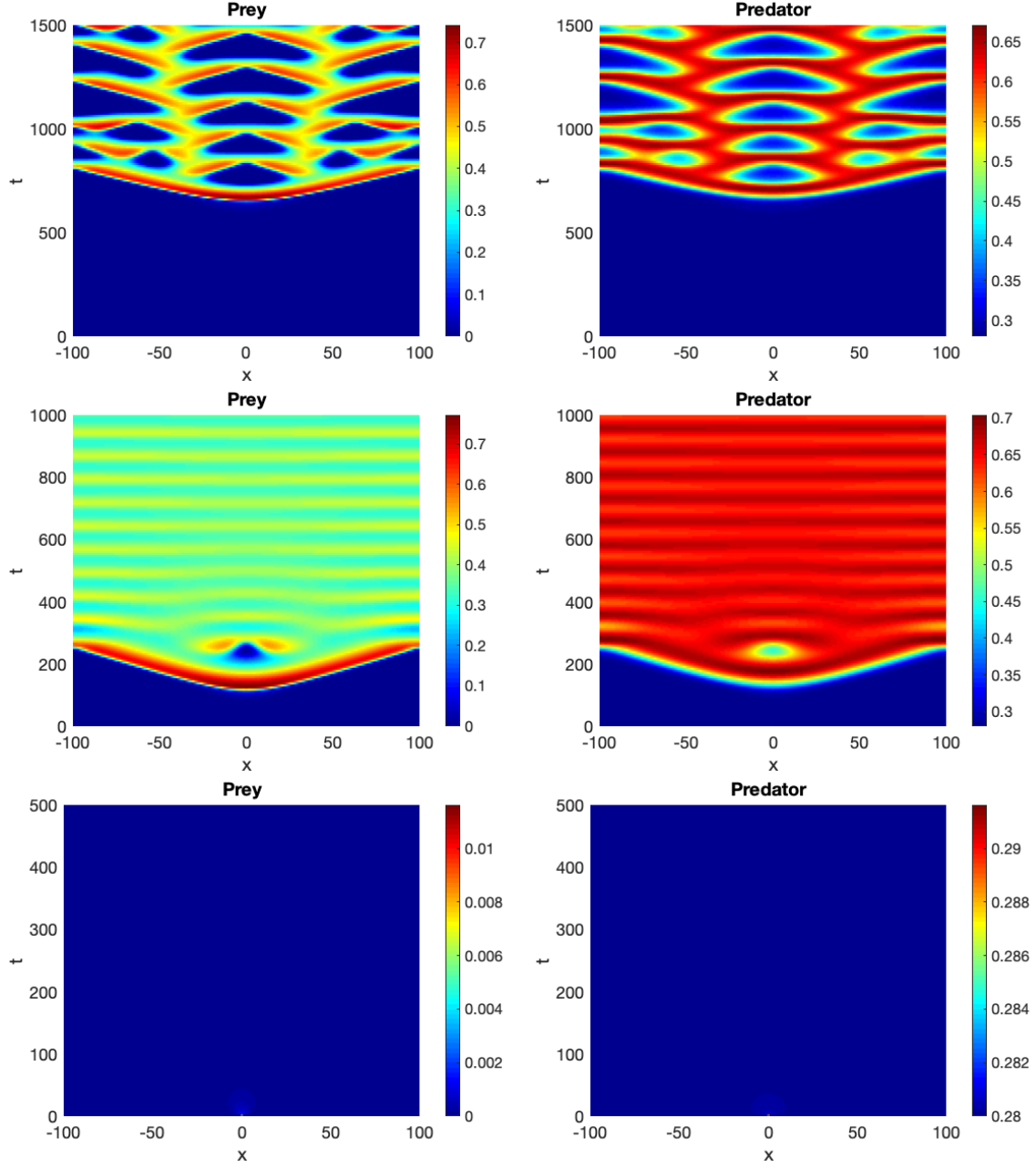


Figure 9: Numerical simulation of system (2) in one-dimensional space with system parameters $(A, C, d) = (0.15, 0.28, 5)$ fixed and initial condition defined in (13). In the top panel $(Q, S) = (0.5, 0.0701)$ and the equilibrium point $(0, C) = (0, 0.28)$ is unstable with respect small wave numbers and wave numbers near λ_d^α , see Figure 8. We observe that the solution is irregular spatial pattern. In the middle panel $(Q, S) = (0.53, 0.0701)$ and the equilibrium point $(0, C) = (0, 0.28)$ is unstable with only respect small wave numbers. We observe that the solution is oscillatory in time with period $250(t)$. In the bottom panel $(Q, S) = (0.575, 0.0701)$ and the equilibrium point $(0, C) = (0, 0.28)$ is stable in the ODE and in the PDE. We observe that the initial condition evolves to $(0, C)$.

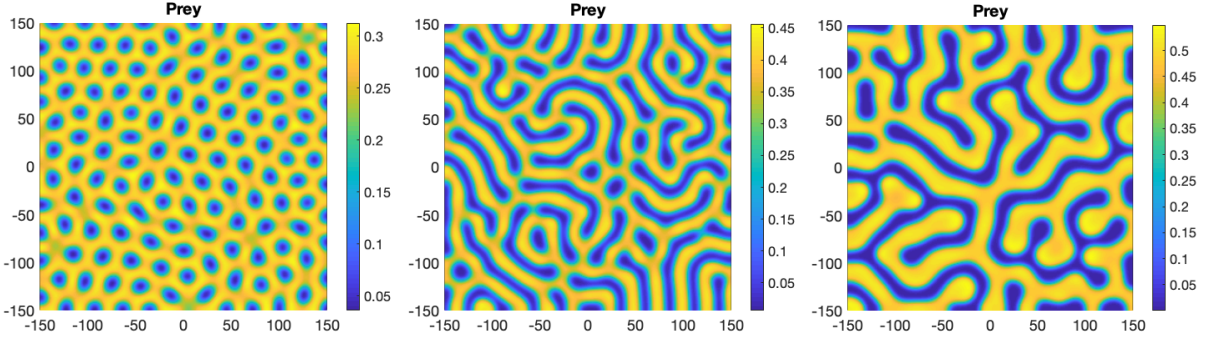


Figure 10: Numerical simulation of the prey population for system (2) in two-dimensional space for initial conditions near to the equilibrium point $(0, C)$. We consider system parameters $(A, C, Q, S) = (0.15, 0.28, 0.575, 0.26)$ fixed and $d = 5$ in the left panel; $d = 9$ in the middle panel; and $d = 55$ in the right panel. We observe the same type of spatial patterns as presented in Figure 7. Note that these patterns are stationary in time.

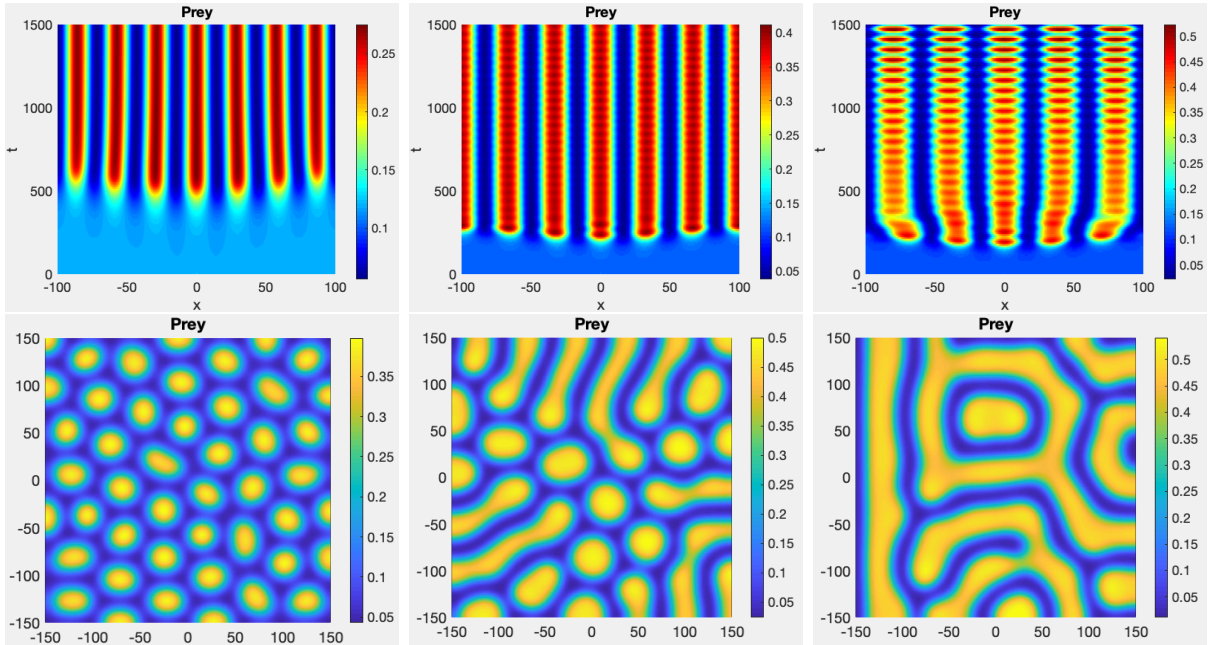


Figure 11: In all cases we consider system parameters $(A, C, Q) = (0.15, 0, 2)$ fixed. On the top panel we show the spatial pattern of system (2) in one-dimensional space with $t = 1500$ and top left panel $S = 0.28$, top middle panel $S = 0.17$, and top right panel $S = 0.13$. On the bottom panel we show the spatial pattern of system (2) in two-dimensional space for the parameter $S = 0.28$ also fixed and $d = 15$ in the bottom left panel; $d = 35$ in the bottom middle panel; and $d = 65$ in the bottom right panel. Note that these Turing patterns are stationary in time.

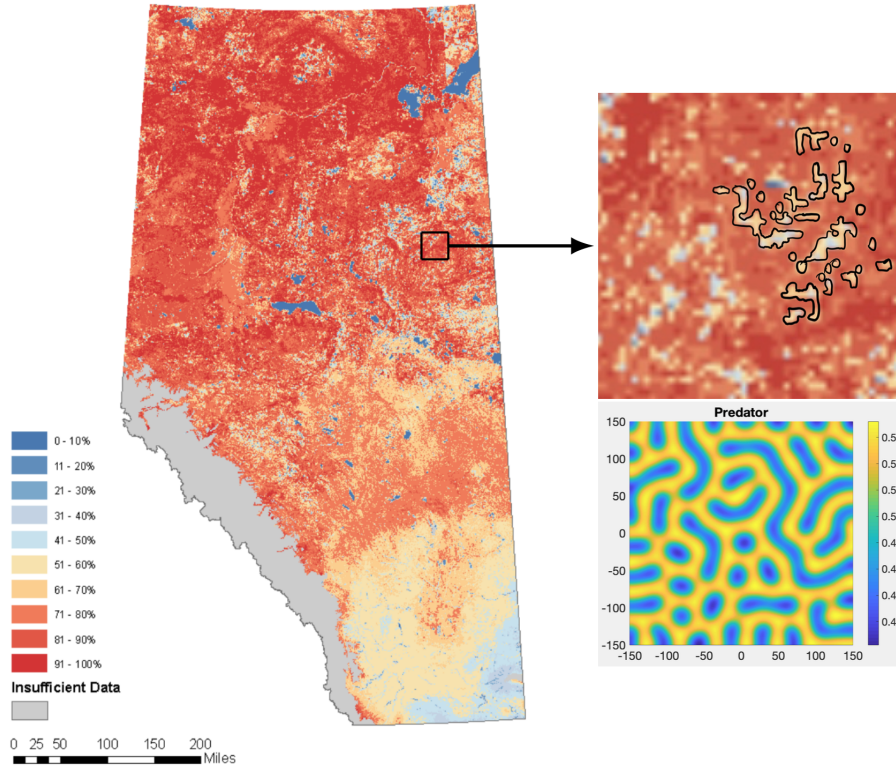


Figure 12: The predicted relative abundance of the weasels and ermine in the forests of the Boreal Forest and Foothills Natural Regions. The map on the left is reproduced with permission from [23].

or stable surrounded by two limit cycles. The global stability of these periodic solutions was studied in [24, 22]. The spatio-temporal analysis of system (2) with $C = 0$ has been studied in [10, 36]. The authors numerically showed that the model supports (Turing) patterns that are either periodic in space and stationary in time; or periodic in both in space and time, see top panel of Figure 11. Moreover, the authors showed that system (2) exhibits different Turing pattern formation in two-dimensional space such as hot-spot patterns, mixture Turing patterns (labyrinthine patterns and hot-spot patterns) and finally only labyrinthine patterns, see bottom panel of Figure 11. We observe that in the model without alternative food the hot spot represent communities in which the prey, respectively the predator, interact (hot spot). While the modified model exhibit areas which are surrounded by communities (cold spot).

The current relative abundance of the weasels observed in the Boreal Forest and Foothills Natural Regions shows that the distribution of this species increases, in general, from approximately 51% up to 100% of the abundance [23]. In Figure 12 we observe that the distribution of weasels form the combination of two types of patterns, i.e. cold-spot patterns and labyrinthine patterns. This is similar to the Turing patterns presented in Figure 7. Since the Turing patterns of the modified model showed in Figure 7 oscillate between 0.4 and 0.55, while the Turing pattern of the original model showed in Figure 11 oscillate between 0 and 0.55. Additionally, the type of patterns presented in the model without alternative food differ with the Turing pattern presented in the original diffusive Holling–Tanner model studied in [10, 36]. In other words, the addition of the alternative food source for the predator in the model generate patterns which better represent the behaviour observed in the Boreal Forest and Foothills Natural Regions. Besides Turing patterns, numerical simulations also suggest that the spatial distribution of the

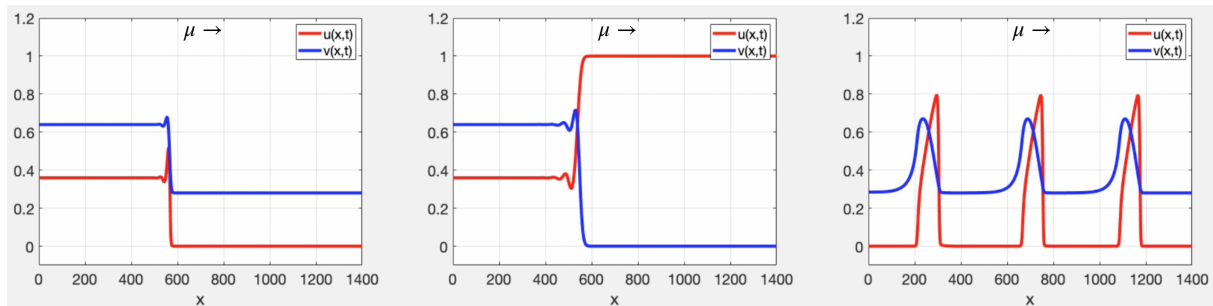


Figure 13: Travelling wave solutions obtained by verifying the scaled intrinsic growth rate of the predator (S) and speed μ . In the left and middle panel $S = 0.18$ and in the right panel $S = 0.03$. In the left panel, the travelling wave represents the invasion of the predator and the death of the prey population, while in the middle panel the travelling wave represents the extinction of predator and the stabilisation of the prey population.

weasels considering an alternative food source better represent the observed distribution of the population in this regions.

Numerical simulation indicate that the modified Holling–Tanner predator–prey model also supports travelling wave solutions. For the system parameter $(d, A, C, Q) = (5, 0.15, 0.28, 0.51)$ fixed we numerically find that if $S = 0.18$ (the scaled intrinsic growth rate of the predator) then there are travelling wave solutions connecting the equilibrium points $(0, C) = (0, 0.28)$ and $(1, 0)$ with $P_2 = (0.36, 0.64)$, see left and middle panel of Figure 13. Additionally, by reducing the parameter $S = 0.03$ we observe that the model also supports wave trains, see right panel of Figure 13. These travelling wave solutions represents the invasion of the predator and the death of the prey population and also the extinction of predator and the stabilisation of the prey population. The analysis of these traveling waves solutions is left as further work.

Acknowledgments

Weasels and Ermine data (2004–2013) from the Alberta Biodiversity Monitoring Institute was used [23], in part, to create Figure 12. More information on the ABMI can be found at: www.abmi.ca.

References

- [1] M. Andersson and S. Erlinge. Influence of predation on rodent populations. *Oikos*, pages 591–597, 1977.
- [2] C. Arancibia-Ibarra. The basins of attraction in a Modified May-Holling-Tanner predator-prey model with Allee effect. *Nonlinear Analysis*, 185:15–28, 2019.
- [3] C. Arancibia-Ibarra, J. Flores, G. Pettet, and P. van Heijster. A holling–tanner predator–prey model with strong allee effect. *International Journal of Bifurcation and Chaos*, 29(11):1–16, 2019.
- [4] C. Arancibia-Ibarra and E. González-Olivares. A modified Leslie–Gower predator–prey model with hyperbolic functional response and Allee effect on prey. *BIOMAT 2010 International Symposium on Mathematical and Computational Biology*, pages 146–162, 2011.

- [5] C. Arancibia-Ibarra and E. González-Olivares. The Holling–Tanner model considering an alternative food for predator. *Proceedings of the 2015 International Conference on Computational and Mathematical Methods in Science and Engineering CMMSE 2015*, pages 130–141, 2015.
- [6] D. Arrowsmith and C. Chapman. Dynamical systems: Differential equations, maps and chaotic behaviour. *Computers and Mathematics with Applications*, 32:132–132, 1996.
- [7] M. Aziz-Alaoui and M. Daher. Boundedness and global stability for a predator–prey model with modified Leslie–Gower and Holling–type II schemes. *Applied Mathematics Letters*, 16:1069–1075, 2003.
- [8] M. Banerjee. Turing and non-Turing patterns in two-dimensional prey-predator models. *Applications of Chaos and Nonlinear Dynamics in Science and Engineering*, 4:257–280, 2015.
- [9] M. Banerjee and S. Banerjee. Turing instabilities and spatio-temporal chaos in ratio-dependent Holling–Tanner model. *Mathematical Biosciences*, 236:64–76, 2012.
- [10] S. Chen and J. Shi. Global stability in a diffusive Holling–Tanner predator–prey model. *Applied Mathematics Letters*, 25:614–618, 2012.
- [11] A. Dhooge, W. Govaerts, and Y. Kuznetsov. Matcont: a matlab package for numerical bifurcation analysis of odes. *ACM Transactions on Mathematical Software (TOMS)*, 29:141–164, 2003.
- [12] S. Erlinge. Predation and noncyclicity in a microtine population in southern Sweden. *Oikos*, pages 347–352, 1987.
- [13] M. Garvie. Finite-Difference Schemes for Reaction–Diffusion Equations Modeling Predator–Prey Interactions in MATLAB. *Bulletin of mathematical biology*, 69:931–956, 2007.
- [14] A. Ghazaryan, V. Manukian, and S. Schecter. Travelling waves in the Holling–Tanner model with weak diffusion. *Proceedings of the Royal Society A: Mathematical, Physical and Engineering Sciences*, 471:1–16, 2015.
- [15] E. González-Olivares, C. Arancibia-Ibarra, A. Rojas-Palma, and B. González-Yañez. Bifurcations and multistability on the May-Holling-Tanner predation model considering alternative food for the predators. *Mathematical Biosciences and Engineering*, 16:4274–4298, 2019.
- [16] E. González-Olivares, C. Arancibia-Ibarra, A. Rojas-Palma, and B. González-Yañez. Dynamics of a modified leslie-gower predation model considering a generalist predator and the hyperbolic functional response. *Mathematical Biosciences and Engineering*, 16:7995–8024, 2019.
- [17] I. Hanski, L. Hansson, and H. Henttonen. Specialist predators, generalist predators, and the microtine rodent cycle. *The Journal of Animal Ecology*, pages 353–367, 1991.
- [18] I. Hanski, H. Henttonen, E. Korpimäki, L. Oksanen, and P. Turchin. Small-rodent dynamics and predation. *Ecology*, 82:1505–1520, 2001.
- [19] I. Hanski, P. Turchin, E. Korpimaki, and H. Henttonen. Population oscillations of boreal rodents: regulation by mustelid predators leads to chaos. *Nature*, 364:232–235, 1993.

- [20] L. Hansson. Competition between rodents in successional stages of taiga forests: *Microtus agrestis* vs. *Clethrionomys glareolus*. *Oikos*, pages 258–266, 1983.
- [21] D. Hooper, F. Chapin, J. Ewel, A. Hector, P. Inchausti, S. Lavorel, J. Lawton, D. Lodge, M. Loreau, and S. Naeem. Effects of biodiversity on ecosystem functioning: a consensus of current knowledge. *Ecological monographs*, 75:3–35, 2005.
- [22] S. B. Hsu and T. W. Huang. Global stability for a class of predator-prey systems. *SIAM Journal on Applied Mathematics*, 55:763–783, 1995.
- [23] Alberta Biodiversity Monitoring Institute. Weasels and ermine (*Mustela*), 2019.
- [24] B. Lisena. Global stability of a periodic holling-tanner predator-prey model. *Mathematical Methods in the Applied Sciences*, 41:3270–3281, 2018.
- [25] Z. Ma and W. Li. Bifurcation analysis on a diffusive Holling–Tanner predator–prey model. *Applied Mathematical Modelling*, 37:4371–4384, 2013.
- [26] H. Malchow, S. Petrovskii, and E. Venturino. *Spatiotemporal patterns in ecology and epidemiology: theory, models, and simulation*. Chapman and Hall/CRC, 2007.
- [27] J. Mathews, K. Fink, et al. *Numerical methods using MATLAB*, volume 4. Pearson Prentice Hall Upper Saddle River, NJ, 2004.
- [28] R. May. *Stability and complexity in model ecosystems*, volume 6 of *Monographs in population biology*. Princeton University Press, Princeton, N.J., 1974.
- [29] R. May. *Stability and complexity in model ecosystems*, volume 6. Princeton university press, 2001.
- [30] R. McDonald, C. Webbon, and S. Harris. The diet of stoats (*Mustela erminea*) and weasels (*Mustela nivalis*) in Great Britain. *Journal of Zoology*, 252:363–371, 2000.
- [31] A. Mondal, A. Pal, and GP. Samanta. On the dynamics of evolutionary Leslie-Gower predator-prey eco-epidemiological model with disease in predator. *Ecological Genetics and Genomics*, 10:1–12, 2019.
- [32] E. Sáez and E. González-Olivares. Dynamics on a predator–prey model. *SIAM Journal on Applied Mathematics*, 59:1867–1878, 1999.
- [33] X. Santos and M. Cheylan. Taxonomic and functional response of a Mediterranean reptile assemblage to a repeated fire regime. *Biological Conservation*, 168:90–98, 2013.
- [34] P. Turchin. *Complex population dynamics: a theoretical/empirical synthesis*, volume 35 of *Monographs in population biology*. Princeton University Press, Princeton, N.J., 2003.
- [35] A. Turing. The chemical basis of morphogenesis. *Philosophical Transactions of the Royal Society*, 237:37–72, 1953.
- [36] W. Wang, Z. Guo, R. Upadhyay, and Y. Lin. Pattern formation in a cross-diffusive Holling-Tanner model. *Discrete Dynamics in Nature and Society*, 2012, 2012.
- [37] D. Wollkind, J. Collings, and J. Logan. Metastability in a temperature–dependent model system for predator–prey mite outbreak interactions on fruit trees. *Bulletin of Mathematical Biology*, 50:379–409, 1988.

- [38] S. Yu. Global asymptotic stability of a predator-prey model with modified Leslie–Gower and Holling–Type II schemes. *Discrete Dynamics in Nature and Society*, 2012:1–8, 2012.
- [39] Z. Zhao, L. Yang, and L. Chen. Impulsive perturbations of a predator–prey system with modified Leslie–Gower and Holling type II schemes. *Journal of Applied Mathematics and Computing*, 35:119–134, 2011.